Advances in Industrial and Manufacturing Engineering 12 (2026) 100191

Contents lists available at ScienceDirect

Advances in Industrial and Manufacturing Engineering

journal homepage: www.sciencedirect.com/journal/advances-in-industrial-and-manufacturing-engineering

Counter pressure enhanced joint strength in spot friction melt bonding of titanium to aluminum

Sanjay C. Krishnamurthy [a,*], Sophie Ryelandt [a], Shavi Agrawal [a], Hosni Idrissi [a], Thaneshan Sapanathan [b], Aude Simar [a,c]

[a] *Institute of Mechanics, Materials and Civil Engineering, Université catholique de Louvain, Louvain La Neuve, 1348, Belgium*
[b] *Curtin Corrosion Centre, Western Australia School of Mines: Mineral, Energy and Chemical Engineering, Curtin University, Western Australia, 6102, Australia*
[c] *WEL Research Institute, Wavre, 1300, Belgium*

ARTICLE INFO

Keywords:
Spot friction melt bonding
Counter-pressure
Dissimilar welding
Titanium
Aluminum
Intermetallic

ABSTRACT

The joining of dissimilar metals offers considerable potential for weight reduction in aerospace structures, especially through the substitution of mechanical fasteners such as screws and rivets with spot-welded joints. Friction Melt Bonding (FMB) is a lap welding technique developed for joining dissimilar metals with large differences in melting temperature. However, achieving sound joints between titanium and aluminum alloys remains challenging due to intermetallic compound formation and uneven material flow. In this study, a modified spot FMB process was proposed to join titanium and aluminum alloys. Particular attention was given to the introduction of a counter-pressure step, aimed at improving the quality of Ti-Al weld joints. Microscopic characterization and mechanical testing were performed on welds produced with and without counter-pressure to assess its role in the joining process. The formation of nano scale Ti-Al intermetallic compounds at the Ti-Al interface assists the joint formation. Fracture surface analysis further confirmed the beneficial effect of counter-pressure in promoting stronger interfacial bonding. These results highlight the critical role of counter-pressure in facilitating interfacial diffusion and consequently, in producing high quality Ti-Al joints through the spot FMB process.

1. Introduction

Titanium (Ti) and aluminum (Al) alloys are widely used in industrial applications due to their good corrosion resistance and high strength-to-weight ratio (Soni et al., 2024). Weight reduction is a continuous demand in the aerospace and automotive industry, striving to reduce fuel consumption (Froes, 1994). Joining dissimilar Ti and Al components offer a promising pathway to achieve this goal, enabling lightweight assemblies without compromising structural integrity or significantly increasing costs (Jain et al., 2019). This approach enables using the right material at the right place - optimizing performance while minimizing material usage. For this purpose, different welding processes adapted for dissimilar metal joining have been developed, including the Friction Melt Bonding (FMB) (Van Der Rest et al., 2014), which is the focus of the present paper and will be presented further in section 2. Until now, FMB had only been validated for steel to Al welds (Jimenez-Mena et al., 2018).

Dissimilar welding of Ti to Al alloys by conventional fusion techniques faces major challenges, including hot cracking (Xue et al., 2021), high residual stress (DebRoy et al., 2026), degradation of base material strength near the weld zone, and formation of thick, brittle intermetallic compounds (IMCs) at the interface (Heidarzadeh et al., 2021). Ti-Al IMCs such as TiAl, $TiAl_3$ and Ti_3Al, reduce ductility of dissimilar welds due to their brittleness (Simar and Avettand-Fènoël, 2017). In particular, weld zone softening and formation of thick Ti-Al IMCs are primary causes of failure in fusion-welded Ti-Al joints (Jiang and Chen, 2019). To address these issues, various strategies have been developed to reduce heat input and improve joint strength. Solid state welding methods, such as friction welding and friction stir welding, alleviate these limitations by operating at lower heat input (Gadakh et al., 2021).

Post-weld rolling has been widely used to fusion welding methods to improve weld quality and reduce distortion (Cozzolino et al., 2017). In friction welding, precisely controlled counter-pressure (upset pressure) is recognized as a key component in achieving high-strength joints with sound metallurgical bonding (Vyas et al., 2021). In dissimilar friction

* Corresponding author. Place Ste-Barbe 2 L5.02.02 Louvain-la-Neuve, 1348, Belgium.
E-mail address: sanjay.krishnamurthy@uclouvain.be (S.C. Krishnamurthy).

https://doi.org/10.1016/j.aime.2026.100191
Received 1 December 2025; Received in revised form 15 April 2026; Accepted 16 April 2026
Available online 16 April 2026

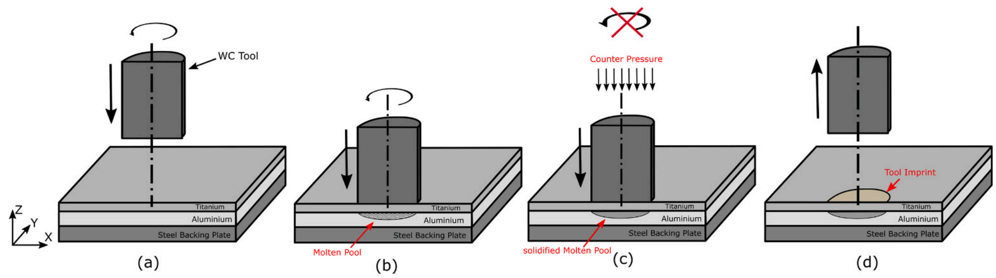

Fig. 1. Schematic illustrations of the counter-pressure assisted Spot Friction Melt Bonding (FMB) process. (a) Flat rotating cylindrical Tungsten Carbide (WC) tool plunging into the Ti surface. (b) Ti-Al lap joint configuration with a steel backing plate, and the heat generated due to friction melts the Al locally beneath the Ti plate, under the tool. (c) Tool rotation stopped while counter-pressure is maintained and solidifying the molten pool during cooling. (d) tool retraction.

welds, counter-pressure promotes uniform thermal dissipation and produce reliable bonding (Gaikwad et al., 2024). Fuji et al. (1997) demonstrated that counter-pressure in Ti to Al friction welds significantly influences joint strength and IMC thickness, with tensile strength increases as friction pressure increases.

Residual stresses are common in dissimilar metal welds (Eisazadeh and Aidun, 2017). Ren et al. (2022) showed that post-weld cold working converted tensile residual stresses to compressive residual stresses at the weld interface in high-strength steel resistance spot welds. Jimenez-Mena et al. (2019) reported tensile residual stresses at the steel-aluminum weld interface in Friction Melt Bonding (FMB) joints, attributed to mismatched thermal expansion coefficients. Such stresses are detrimental as they promote crack growth and premature failure in dissimilar welds (Correia et al., 2021).

This study proposed a modified spot FMB process for joining dissimilar Ti-Al alloys. The research focuses on quantifying the influence of counter-pressure on the thermal field, interfacial reactions and microstructural evolution during welding. Ti-Al spot FMB joints produced with and without counter-pressure are compared, and their mechanical behavior under shear loading, along with the corresponding failure mechanisms is systematically analyzed and discussed.

2. Modified spot friction melt bonding (FMB) process

FMB is patented at UCLouvain (Jacques et al., 2012) for joining dissimilar metals with large differences in melting temperatures. The FMB process has been widely studied for dissimilar linear steel and Al welds (Jimenez-Mena, 2018) but never reported for spot welding. The current study examines the significance of a modified spot FMB process for joining Ti and Al. The various stages of the spot FMB process are described below in (a) - (d) and are illustrated in Fig. 1.

a) Tool plunging:

In the spot FMB process, the high melting point metal (Ti) is placed over the low melting point metal (Al). A flat, rotating cylindrical Tungsten Carbide tool is slightly plunged into the Ti surface which starts to generate heat due to friction (Fig. 1a).

b) Frictional heat generation:

The heat generated at the top surface of Ti is transmitted to the interface, locally melting the Al (Fig. 1b). Al reacts with Ti at high temperatures generally forming intermetallic compounds (IMCs), which facilitates bond formation.

c) Application of post-weld counter-pressure:

In the classical FMB process, the tool is removed after the frictional step. In the modified post weld “counter-pressure” strategy, the tool rotation is stopped while maintaining contact force (Fig. 1c). The counter-pressure is applied for 30 s to promote enhanced bond

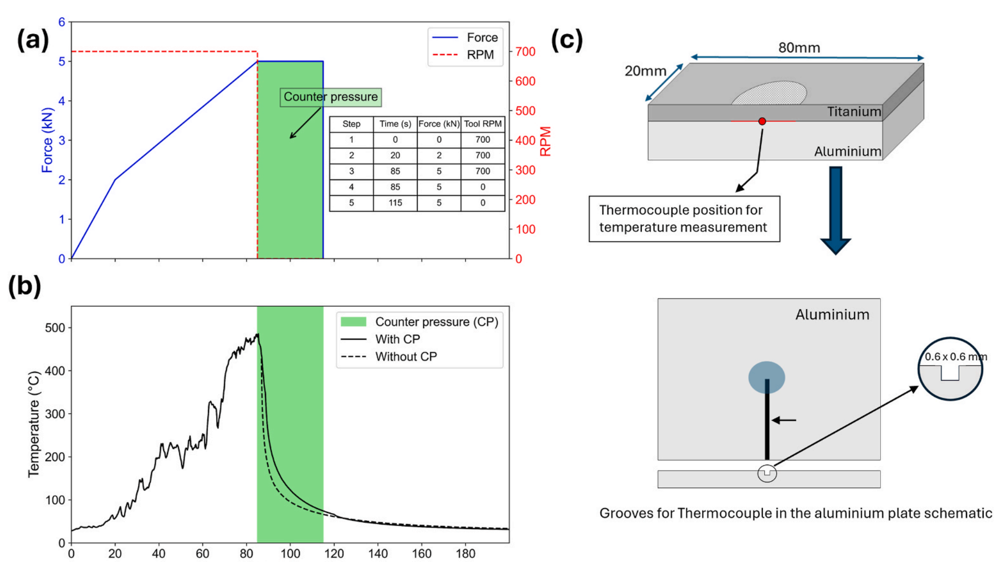

Fig. 2. (a) Optimized process parameter: Force and rotation speed versus time plot. The green region highlights the post weld counter-pressure step applied at the end of the plunging stage (inset table: detailed selected process parameters). (b) Temperature evolution at the Ti-Al weld interface during spot FMB. (c) Schematic illustration showing thermocouple location at the weld interface, embedded in the Al plate by machining a groove.

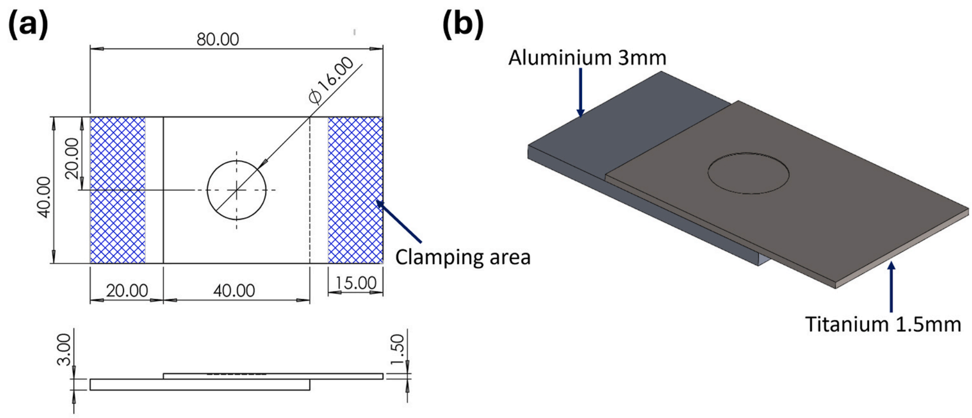

Fig. 3. (a)The schematic of Lap shear test sample in 2D with dimensions (b) 3D view of the Lap shear test sample.

formation.

d) Tool retracting:

After the counter-pressure application, the tool is retracted, leaving a welded Ti-Al joint (Fig. 1d).

3. Materials and methods

3.1. Materials

Commercially pure Ti Grade 4 sheets (1.5 mm thick) and 6061-T6 rolled Al alloy sheets (3 mm thick) are used in this study. The weld samples measured 80 mm and 40 mm for length and width, respectively. Prior to welding, the coupons were polished with 1200-grit SiC paper and degreased with acetone. Detailed alloy compositions, measured using inductively coupled plasma (ICP-OES) analysis, and mechanical properties of Ti Grade-4 and Al 6061-T6, obtained from tensile testing in accordance with ASTM E8M, are provided in Supplementary S1.

3.2. Process parameters and temperature measurements

The spot FMB welding process was performed using force-controlled tool plunging mode with a rotation speed of 700 rpm. Optimal process parameters were determined experimentally. The parameter optimization procedure is detailed in Supplementary S2, which includes the staircase methodology used for parameter selection, as well as the limitations associated with the narrow process window encountered in this study. The selected process parameters based on this procedure are listed in the inset table in Fig. 2a. Despite optimization, occasional plate separation occurred upon removal of the plates from the fixture. To address this issue, an application of post-weld counter-pressure (as detailed in section 2) was introduced in which tool retraction was delayed by maintaining contact for 30s. The 30-s dwell time was determined based on the time required for the weld interface to cool to 50 °C (Fig. 2b). This strategy allows for thermal relaxation of the weld under sustained force, mitigating immediate weld separation caused by the mismatched thermal expansion of Ti and Al. This strategy significantly improved repeatability in producing successful Ti-Al spot FMB welds.

This adopted counter-pressure approach and selected process parameters are summarized in Fig. 2a. Temperature evolution during welding, with and without counter-pressure, was measured at the weld interface using a K-type thermocouple embedded in the Al plate. The results are shown in Fig. 2b, and thermocouple positioning is illustrated in Fig. 2c.

3.3. Microstructure characterization

The welds were dissected through their centers using a micro-cutting machine. Microstructural analysis of the weld interface and fractography of lap shear test-failed samples were performed using a Keyence VHX-7000 digital optical microscope (OM) and a Zeiss Ultra 55 scanning electron microscope (SEM) equipped with an Energy Dispersive X-ray Spectroscopy (EDX) detector. The weld cross-sections were polished to a 0.04 μm finish and etched with Keller's reagent (2.5% HNO_3, 1.5% HCl, 1% HF and balance water) to evaluate the effect of welding process on the base material microstructure. For transmission electron microscopy (TEM), thin foils were extracted from the weld center using focused ion beam (FIB) milling. TEM characterization was conducted using a Talos HR-TEM operated at 200 kV. Phase identification at the Ti–Al interface was carried out using FFT patterns obtained from selected regions and comparing them with simulated patterns for the corresponding zone axes, ensuring confident identification.

3.4. Mechanical characterization

The spot FMB welded samples were subjected to single lap shear testing as described in detail by (Jimenez-Mena et al., 2021). The shear test coupons were prepared from the weld using electrical discharge machining (EDM). To avoid bending effects commonly observed in longer lap shear specimens (Özel et al., 2004), the overall specimen length was shortened, ensuring a dominant shear mode. The dimensions of the lap shear test samples for the spot FMB Ti-Al welds used in this study are shown in Fig. 3.

Among the ten spot FMB Ti-Al welds produced without counter-pressure, only one survived the process for mechanical testing. Most of the welds delaminated during removal from the fixture. A few of the surviving welds were subjected to machining using EDM. However, only one weld remained intact after EDM and was suitable for lap shear tensile testing. This sample was carefully handled to preserve its integrity for strength validation.

The lap shear test was conducted at a crosshead speed of 0.5 mm/min. Three samples were tested for with counter-pressure condition. The failure stress was calculated based on the bonded area obtained from the fractography observations of the Ti-Al welds. The fracture surface measurement methodology as well as the methodology used to determine the actual bonded area for stress calculation are provided in Supplementary S3. Vickers micro-hardness measurements were performed on the weld mid-section using an Emco-Test Durascan 5G equipment under a 0.2 kg load with a 10 s dwell time. Indentations were made at 0.3 mm intervals in Al and at intervals of 0.2 mm in Ti along both X and Z directions (direction convention see Fig. 1).

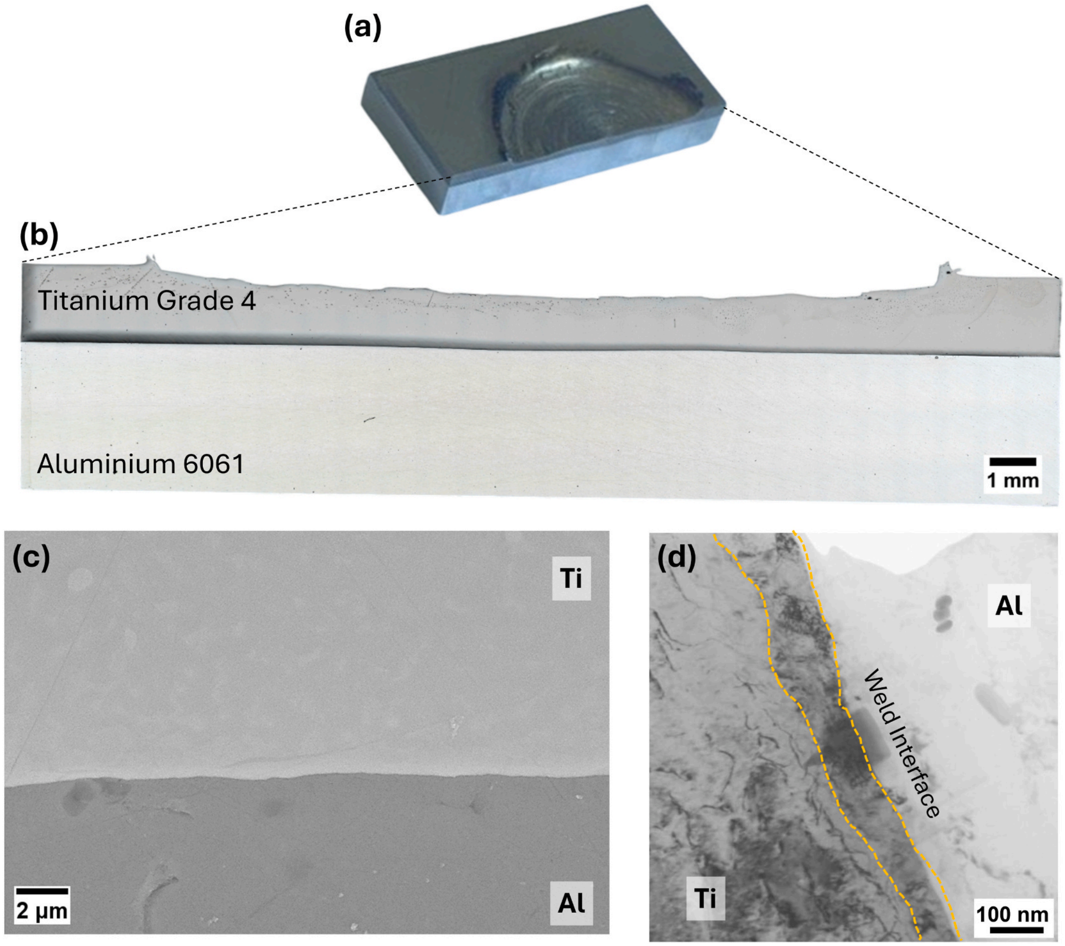

Fig. 4. (a) Image of the spot FMB Ti–Al weld sample sectioned through the weld mid-section; (b) optical micrograph of the weld interface; (c) SEM and (d) BF-TEM observations of the spot FMB weld between Titanium Grade 4 and Aluminum 6061 with counter-pressure.

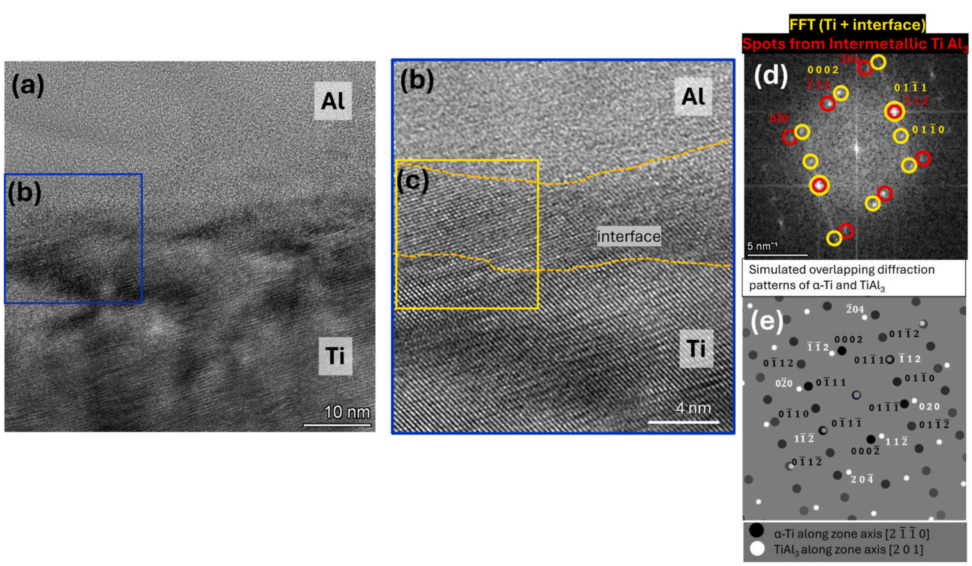

Fig. 5. (a) High-resolution TEM (HRTEM) image of the weld interface; (b) Magnified HR-TEM image of the diffused weld interface; (c) HR-TEM region of the weld interface from which Fast Fourier Transformed (FFT) pattern has been taken; (d) Indexed FFT spots identified as α-Ti and $TiAl_3$ in the diffused weld interface region along Zone Axis (ZA) $[2\bar{1}\bar{1}0]$ Ti//[201]$TiAl_3$ corresponding to c; and (e) Simulated overlapping diffraction pattens of α -Ti and Ti Al_3 along Zone Axis (ZA) $[2\bar{1}\bar{1}0]$ Ti and [201]$TiAl_{3.}$. Note: Spots encircled in red correspond to Ti Al_3, while spots encircled in yellow correspond to α -Ti in d.

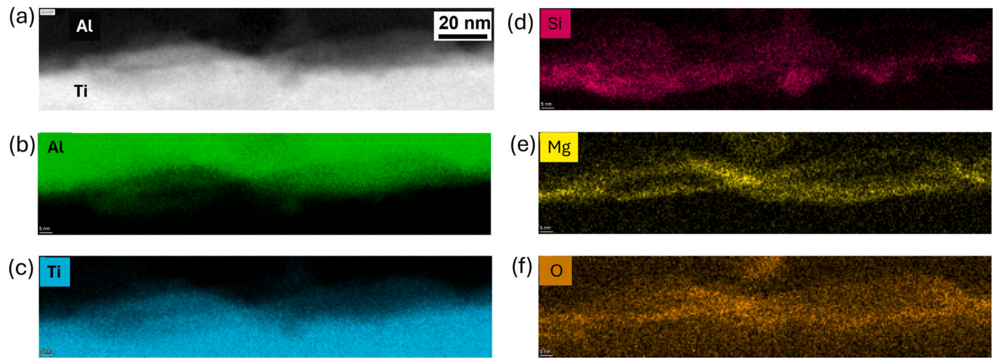

Fig. 6. (a) STEM image of the FMB spot Ti–Al weld interface processed under counter-pressure, with corresponding EDX maps of (b) Al, (c) Ti, (d) Si, (e) Mg, and (f) O, showing elemental segregation across the weld interface.

4. Results and discussion

4.1. Joint profile and microscopy

The cross-section and interface microstructure of the FMB Ti-Al spot weld with counter-pressure, observed at different scales, are shown in Fig. 4. The overall weld cross section in Fig. 4a and b reveals significant plastic deformation on the top of the Ti surface, induced by the tool contact during processing. A straight and well-defined interface between Ti and Al is observed. The higher-magnification SEM image in Fig. 4c further confirm a clean weld interface without the formation of a thick interfacial reaction layer or continuous intermetallic compounds (IMCs). In contrast, the BF-TEM micrograph of Fig. 4d, a thin layer exhibiting distinct diffraction contrast can be observed at the interface.

To gain deeper insight into the joining mechanism, the Ti-Al weld interface was analyzed by HR-TEM, as shown in Fig. 5a and b, along with spots of Fast Fourier Transformed (FFT) pattern to identify interfacial phases. The HR-TEM images reveal a nanoscale diffused interface. The overlapping FFT pattern of the interfacial region (inset Fig. 5c) shows diffraction spots corresponding to α-Ti, along with additional spots that were indexed to $TiAl_3$ (Fig. 5d). Simulated overlapping diffraction patterns of α -Ti and Ti Al_3 along Zone Axis (ZA) $[2\bar{1}\bar{1}0]$ Ti and [201] $TiAl_3$ is shown in Fig. 5e. The FFT indexed spots confirm that the FMB Ti-Al spot weld interface consists of a diffused Ti-Al transition region with the formation of nanoscale $TiAl_3$ intermetallic compounds. The average thickness of this interfacial layer was measured to be 5.5 ± 0.8 nm. Overlapping FFT patterns of α-Ti and $TiAl_3$ (Fig. 5d) also provide the information regarding crystallographic orientation relationship between these Ti and $TiAl_3$ where $[2\bar{1}\bar{1}0]$ Ti//[201]$TiAl_3$, $(01\bar{1}1)$ Ti//$(\bar{1}12)$ $TiAl_3$ and $(0\bar{1}1\bar{1})$ Ti//$(1\bar{1}\bar{2})$$TiAl_3$. Liu et al. (2021) reported the preferential nucleation of $TiAl_3$ on the Ti side of the interface, which was attributed to the faster diffusion of Al compared to Ti at temperatures near 500 °C.

A detailed STEM-EDX analysis of the Ti-Al FMB spot weld interface, shown in Fig. 6, reveals the segregation of diffusing alloying elements such as Si and Mg. Such segregation of Si and Mg is commonly reported at diffusion-bonded weld interfaces of Ti and Al alloys (Li et al., 2020). Notably, in Fig. 6d, Si-enriched segregation is evident near the Ti/$TiAl_3$ interfacial diffusion zone, while in Fig. 6e, Mg segregation appears further toward the Al side of the diffused interface. Liu et al. (2022)

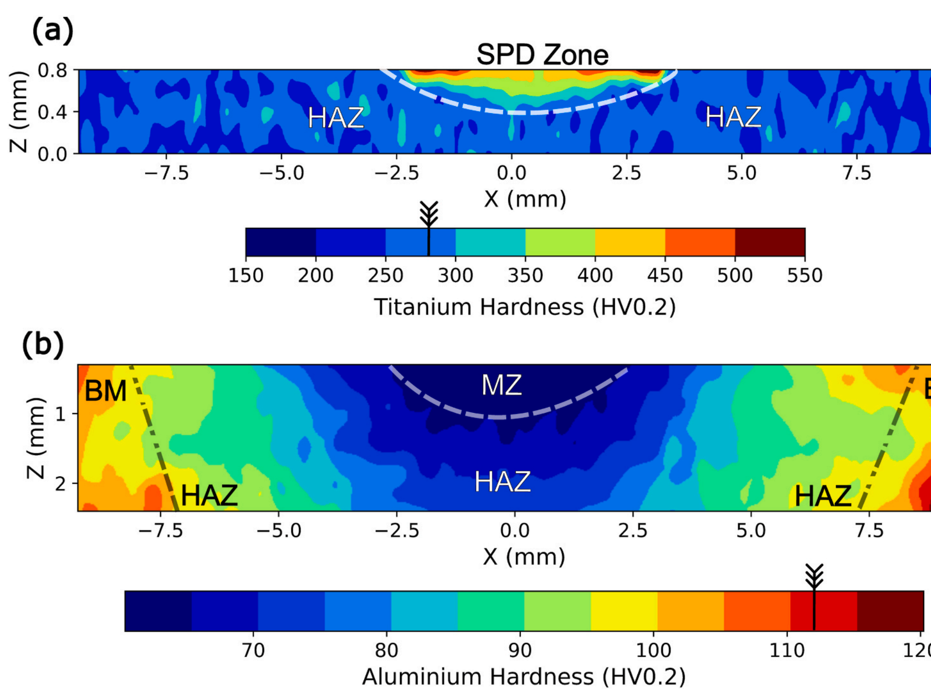

Fig. 7. Micro-hardness distribution maps at spot FMB weld center for (a) titanium and (b) aluminum, showing the processed and heat-affected zones. The arrows in the hardness legend indicate the base material hardness values, providing a reference to aid interpretation of the results. (SPD = severe plastic deformation, BM = base material, MZ = melt zone, HAZ = heat-affected zone).

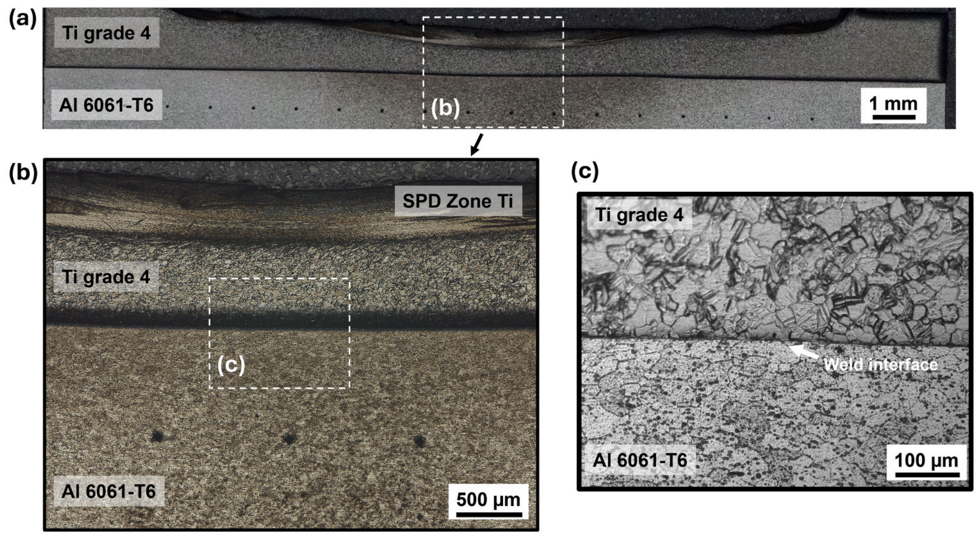

Fig. 8. Etched cross-sections of spot FMB Ti-Al weld with counter-pressure: (a) optical micrograph of the full weld cross-section (b) enlarged view of the weld center highlighting the severe plastic deformation (SPD) Zone in Ti Grade 4 (c) enlarged view of the Ti-Al weld interface.

reported similar behavior at the Ti-Al interface and attributed this preferential segregation to the atomic sizes of the elements. Specifically, the smaller atomic radii of Si (0.117 nm) and Al (0.143 nm), compared with Mg (0.160 nm), result in a lower activation energy for diffusion. In addition, Si and Ti exhibit significantly negative chemical mixing enthalpy ($\Delta H_{mix}^{Ti-Si} = -66$ kJ/mol), leading to strong chemical interactions (Zhang et al., 2019). Accordingly, in Fig. 6d, Si is observed to diffuse further towards the Ti side, exhibiting greater enrichment in this region compared to Al, as shown in Fig. 6b.

4.2. Mechanical performance of the welds

4.2.1. Microhardness distribution

Hardness mapping was performed across the spot FMB weld section for both Ti and Al to assess the effect of the welding process in the processed zone, heat affected zones (HAZ) and the base materials. The measured hardness values of the base materials were 281 ± 10 HV0.2 for Grade 4 Ti and 112 ± 4 HV0.2 for 6061-T6 Al. The hardness distributions for the spot FMB Ti-Al welds are presented in Fig. 7.

The Ti surface at the weld center (Fig. 7a) where the tool was in direct contact during processing, exhibit higher hardness values (>300 HV 0.2) than that of base Ti alloy. Below this zone is the HAZ, which does not show any significant change in hardness, indicating limited thermal influence on the microstructure during the FMB process. The corresponding region of higher hardness value (>300 HV 0.2) near the tool contact surface (Fig. 7a) is also visible in the etched cross-section of the FMB Ti-Al (Fig. 8b). This increased hardness region at the weld center corresponds to a severely plastically deformed (SPD) zone with fine grains. Li et al. (2014) demonstrated that intense shear plastic deformation can significantly increase the strength of commercially pure (CP) Ti. Therefore, the observed hardness increase at tool contact region of Ti can be attributed to substantial grain refinement induced by SPD during the spot FMB process. However, this localized hardening does not extend up to the weld interface.

In Al (Fig. 7b), the weld center near the interface presents a hardness reduction to approximately 60 HV0.2, corresponding to the melted zone. In comparison, the surrounding HAZ zone exhibits a hardness value of around 80-90 HV0.2. This gradient is mainly due to the transformation of fine coherent β″ metastable precipitates in the T6 state, which coarsen into β’ and β precipitates during the thermal cycle (Jonckheere et al., 2013). These coarser precipitates are incoherent with the Al matrix, leading to reduced hardness on the Al side in Ti-Al FMB welds.

4.2.2. Effect of counter-pressure on the joint strength

Lap shear tests were conducted to evaluate the joint strength of

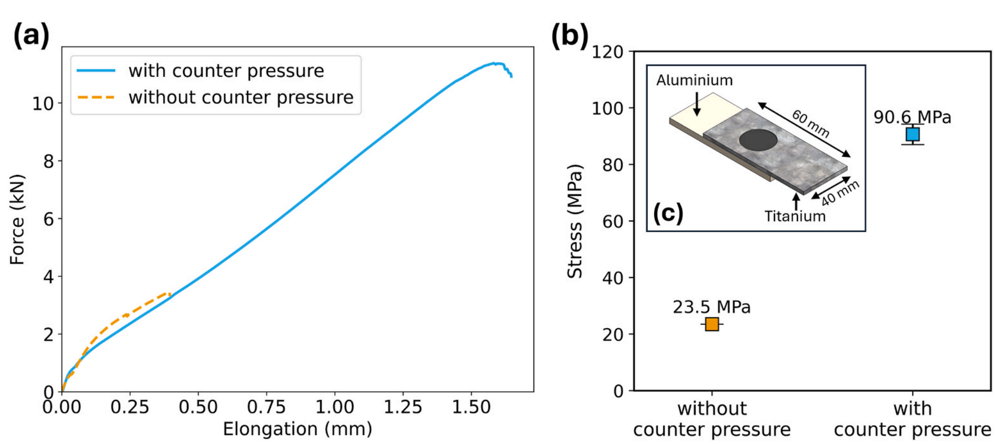

Fig. 9. (a) Representative force-elongation curves from single lap shear test of spot FMB Ti-Al welds, with and without counter-pressure and (b) comparison of calculated stresses (c) inset: 3D schematic illustration of a lap shear test sample.

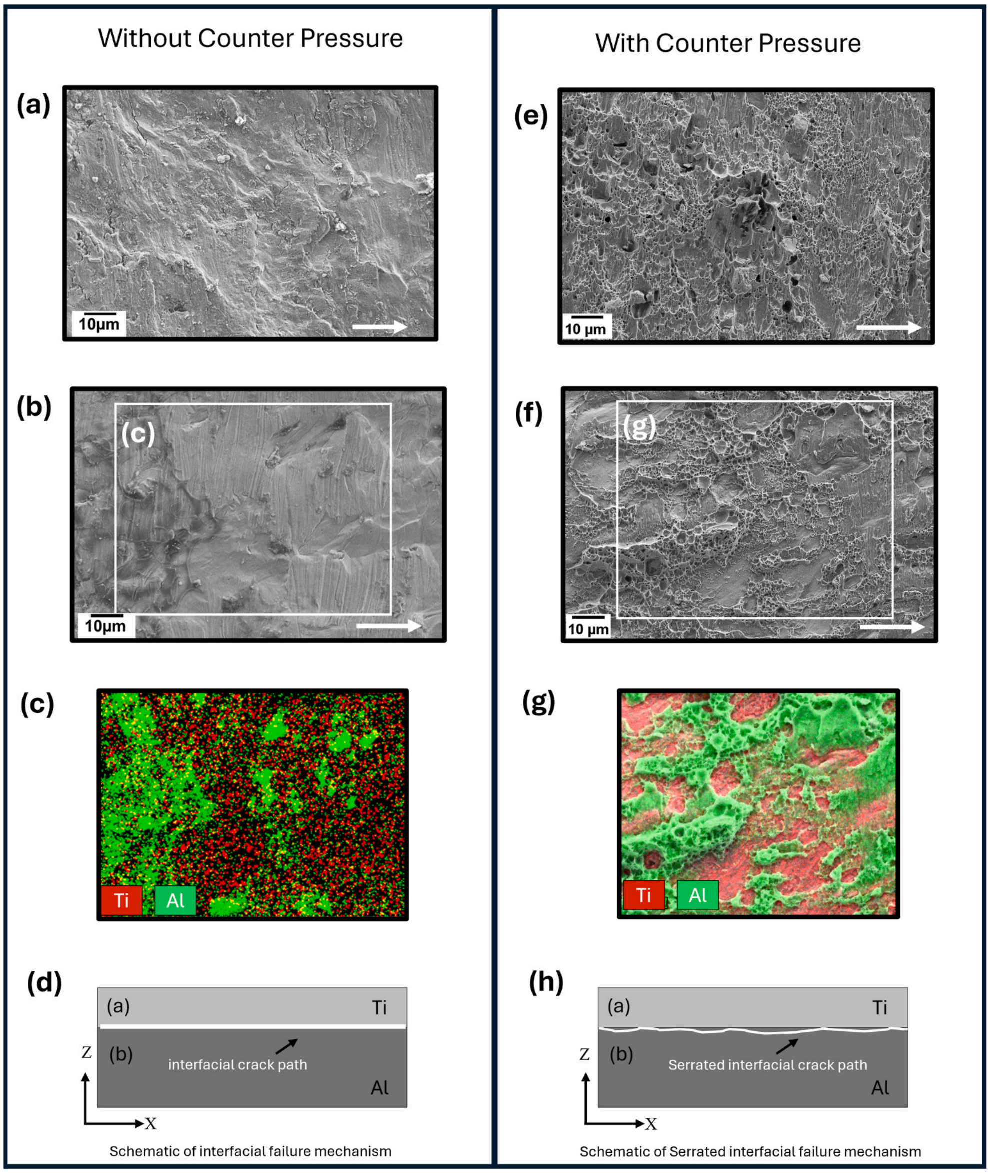

Fig. 10. Fractography of failure surfaces (in the X-Y plane) after the single lap shear test corresponding to the spot weld FMB specimen (a) Aluminum surface without counter-pressure and (b) Titanium surface without counter-pressure showing brittle cleavage features; (c) EDX map on the titanium side surface corresponding to the box in b; (d) schematic representation of crack propagation in the sample without counter-pressure based on fractography.(e) Fractography observations of failure surfaces (in the X-Y plane) after the single lap shear test corresponding to the spot weld FMB specimen with counter-pressure on the aluminum surface and (f) Titanium surface with white arrows indicating the direction of crack propagation; (g) EDX map of the titanium side surface corresponding to the box in f; and (h) schematic representation of crack propagation in the sample with counter-pressure based on fractography.

dissimilar Ti-Al spot FMB welds produced with and without counter-pressure. For samples welded without counter-pressure, only those that did not separate spontaneously were tested (see section 3.4 for details). The force-elongation response is shown in Fig. 9a, and the corresponding stress values obtained by normalizing the force by contact area, is presented in Fig. 9b.

The results indicate that spot FMB Ti-Al welds produced with counter-pressure exhibited an average joint strength of 90.6 ± 5 MPa, whereas welds without counter-pressure showed stresses ranging from 0 MPa (corresponding to unwelded samples) to 23.5 MPa. In the latter case, most welds failed prematurely, and only one sample remained sufficiently intact for tensile testing, highlighting the low quality and low reproducibility of joints produced without counter-pressure. Due to this limitation, a direct quantitative comparison between the two conditions is constrained. Nevertheless, the application of counter-pressure resulted in a substantial and systematic increase in joint strength, demonstrating its critical role in improving weld integrity and mechanical performance in dissimilar Ti-Al FMB joints.

4.2.3. Fractography and crack propagation

The fracture surfaces after lap shear testing were examined to identify the failure mechanisms. Fig. 10 shows the spot FMB welds produced without counter-pressure (Fig. 10a and b) and with counter-pressure (Fig. 10e and f). In the absence of counter-pressure, the Al fracture surface (Fig. 10a) exhibits a cleavage river pattern, which is also observed on the Ti side (Fig. 10b). These features are characteristics of brittle interfacial cleavage fracture. Qualitative EDX mapping (Fig. 10c) further confirmed the presence of Al ridges on the Ti side fracture surface (Fig. 10b). A schematic illustration of this interfacial failure mode in spot FMB welds without counter-pressure is presented in Fig. 10d.

In contrast, the fracture surfaces of the spot FMB weld samples produced with counter-pressure (Fig. 10e–h) exhibit distinct ductile

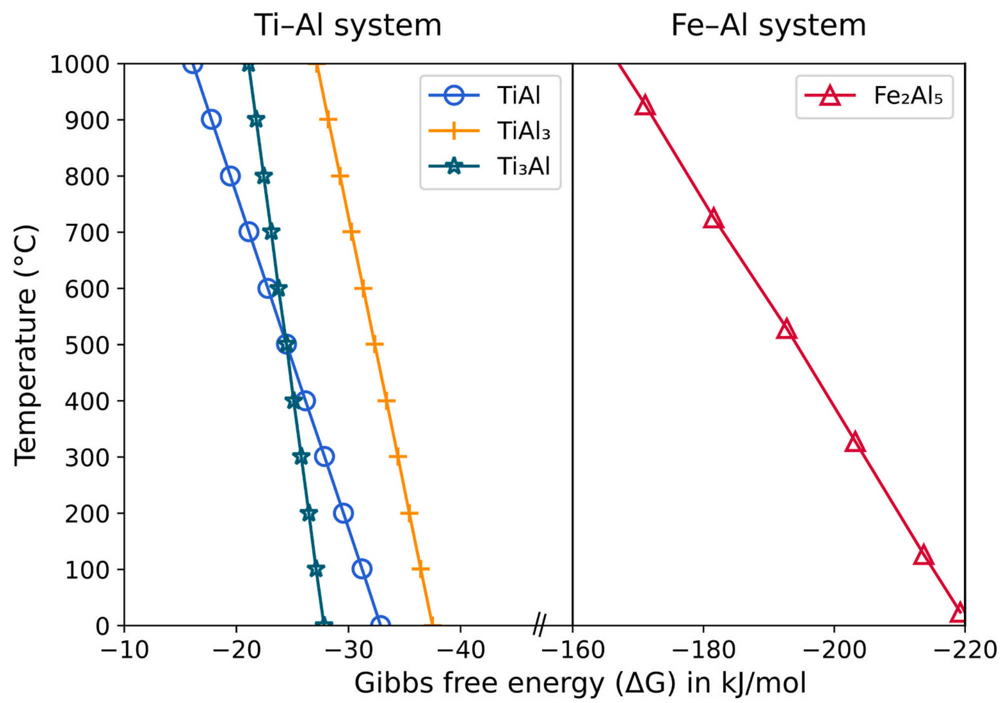

Fig. 11. Gibbs Free energy (ΔG) of formation of different Fe-Al and Ti–Al IMCs as a function of temperature (based on data from (Dezellus et al., 2021; Pretorius et al., 1991)).

features. Ductile dimples are clearly visible on the Al surface (Fig. 10e), while the Ti side (Fig. 10f) shows a mixed morphology of cleavage and ductile dimple regions. Qualitative EDX mapping (Fig. 10g) confirmed that cleavage regions corresponded to Ti signals, and the dimple-rich zones were associated with Al signals. These observations suggest a serrated interfacial crack failure, where cracks deviate into the lower hardness Al (Fig. 10h).

Akisanya et al. (Akisanya and Fleck, 1992) reported that the serrated interfacial cracks are more common in the presence of high residual stresses. Jimenez-Mena et al. (2019) also observed significant tensile residual stress at the weld interface in steel-Al FMB weld joints. Cozzolino et al. (2017) demonstrated that post-weld rolling could convert tensile residual stresses to compressive, aligning with the present findings. This explains the change in failure mechanisms and emphasizes the crucial role of counter-pressure in producing high-quality Ti-Al welds.

The difference in failure mechanism and increase in joint strength can also be linked to the formation of a thin (nanoscale level) IMC at the weld interface. Jimenez-Mena et al. (2021) reported that in dissimilar steel-Al FMB welds, a thick intermetallic (IMC) layer restricted crack propagation to the interface, resulting in cleavage facets and brittle fracture within the interfacial IMC layer. In contrast, as shown in Fig. 10, the presence of a nanoscale-thin IMC layer can lead either to brittle interfacial failure or to crack deviation into the lower hardness Al. Nevertheless, failure is still limited to the region near the weld interface. The formation of IMCs at weld interface can be rationalized based on Gibbs free energy calculations (Sujata et al., 1997).

The formation of IMCs at a bi-metal interface is a dynamic, non-equilibrium process. Fig. 11 compares the Gibbs free energy (ΔG) of Fe-Al and Ti-Al systems to highlight differences in IMC thickness and growth behavior. In the Fe-Al system, the relatively lower ΔG provides a strong thermodynamic driving force, enabling rapid nucleation and growth of IMCs to the microscale. In contrast, the Ti-Al system has a higher ΔG, which reduces the driving force for reaction (Pretorius et al., 1991). This limitation is further enhanced by the inherently slower interdiffusion between Ti and Al and the higher activation energies required for interface reactions (Dezellus et al., 2021). As a result, IMC growth in the Ti-Al joints produced by FMB remains limited, leading to nanoscale IMC layers (Fig. 5). This combined thermodynamic and kinetic interplay explains the pronounced difference in IMC thickness between the Fe-Al and Ti-Al systems.

In summary, the introduction of counter-pressure in the spot FMB process plays a crucial role in achieving high-quality Ti-Al weld joints, which can be highlighted in three key aspects:

The applied pressure during welding promotes localized plastic deformation at the weld interface, increasing the density of dislocations and vacancies in softer aluminum (Karfoul and Tatlock, 2019). These defects are well known fast diffusion pathways that facilitate diffusion assisted IMC formation in Al (Robson, 2020). Although direct quantification of diffusion enhancement is beyond the scope of the present study, this mechanism is consistent with diffusion assisted IMC formation reported in pressure assisted solid-state joining of Ti-Al welds in the literature (Grassel et al., 2025).

The application of post weld counter-pressure step secures the interface during tool retraction, suppressing the interfacial separation observed in welds produced without counter-pressure. Maintaining this pressure during the early cooling period is also expected to promote thermal stress relaxation, thereby potentially reducing the formation of tensile residual stresses (Pragana et al., 2021) that typically arise from the mismatch in thermal expansion between Ti and Al (Zheng et al., 2025). It should be noted that the residual stress effects discussed here are inferred based on the observed behavior and supporting literature, as no direct residual stress measurements were performed in the present study. A comprehensive residual stress analysis is currently underway and forms part of a follow-up study.

This ensures intimate contact between Ti and Al directly beneath the tool, enabling reaction/diffusion and continuous IMC formation, as evidenced in the high resolution TEM observations (Figs. 4 and 5). By providing extended dwell time and maintaining interface stability, the counter-pressure strategy effectively enhances diffusion-driven nanoscale IMC formation (5.5 ± 0.8 nm), thereby enabling to produce high quality Ti-Al weld joints in the proposed spot FMB process.

To further contextualize the performance of the proposed spot FMB process for Ti-Al lap joints, the lap shear strength of the joints produced in this study was compared with literature reported values for

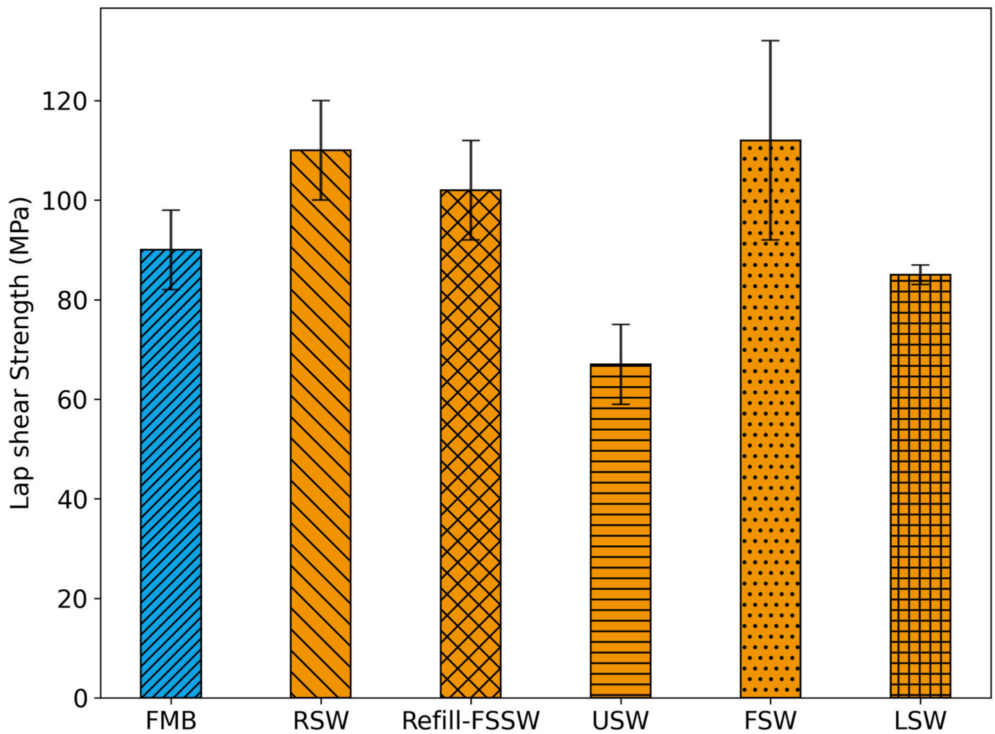

Fig. 12. Comparison of lap shear strength of Ti–Al lap joints produced by the FMB process in the current study with other welding processes reported in the literature: resistance spot welding (RSW) (Li et al., 2015), Refill friction stir spot welding (Refill-FSSW) (Nan et al., 2025; Plaine et al., 2015), ultrasonic welding (USW) (Zhang et al., 2016), friction stir welding (FSW) (Chen and Yazdanian, 2015), and laser spot welding (LSW) (Fernandes et al., 2023). Error bars represent the variability in reported and measured strength. Note: The base materials used in the literature are Ti-6Al-4V and 6xxx series aluminum alloys.

alternative welding methods for Ti and Al (Ti-6Al-4V and 6xxx-series Al alloys) in lap joint configurations, including resistance spot welding (RSW) (Li et al., 2015), Refill friction stir spot welding (Refill-FSSW) (Nan et al., 2025; Plaine et al., 2015), ultrasonic welding (USW) (Zhang et al., 2016), friction stir welding (FSW) (Chen and Yazdanian, 2015), and laser spot welding (LSW) (Fernandes et al., 2023) (Fig. 12). The FMB joints exhibit competitive or superior strength compared to existing welding methods, demonstrating that the combination of counter-pressure and nanoscale IMC formation not only enhances interfacial integrity but also produces mechanically robust joints. Notably, the process allows weld access through the Ti side, a distinct advantage in aerospace applications where assembly constraints limit tool accessibility. As a semi-solid state welding technique, spot FMB leverages localized plastic deformation and diffusion-assisted bonding, offering a versatile approach for developing high-performance Ti-Al joints. These results position FMB as a promising alternative to conventional solid-state and fusion welding methods, capable of meeting stringent mechanical and geometric requirements in advanced engineering applications.

5. Conclusions

In this study, an innovative post-weld counter-pressure strategy was used for producing successful dissimilar Ti and Al weld in a spot Friction Melt Bonding (FMB) process. The joint quality is systematically evaluated through detailed microstructural and mechanical characterizations. The results demonstrate that high-strength Ti-Al spot welds can be successfully produced using the modified spot FMB process. The considerable improvement of interface integrity is promoted by nanoscale intermetallic compound (IMC) formation driven by the favorable thermodynamic conditions.

The application of counter-pressure significantly enhances atomic diffusion across the Ti-Al interface, promoting the formation of nanoscale Ti-Al intermetallic compounds that contribute to a stronger metallurgical bond. As a result, the use of counter-pressure shifts the failure mechanism from interfacial brittle failure (in conventional FMB welds without counter-pressure) to mixed or even ductile failure modes.

CRediT authorship contribution statement

Sanjay C. Krishnamurthy: Writing – original draft, Visualization, Validation, Project administration, Methodology, Investigation, Funding acquisition, Formal analysis, Conceptualization. **Sophie Ryelandt:** Writing – review & editing, Validation, Methodology, Investigation. **Shavi Agrawal:** Writing – review & editing, Visualization, Methodology, Investigation, Formal analysis. **Hosni Idrissi:** Writing – review & editing, Validation, Resources. **Thaneshan Sapanathan:** Writing – review & editing, Validation, Conceptualization. **Aude Simar:** Writing – review & editing, Validation, Supervision, Resources, Project administration, Methodology, Funding acquisition, Conceptualization.

Declaration of competing interest

The authors declare that they have no known competing financial interests or personal relationships that could have appeared to influence the work reported in this paper.

Acknowledgement

The authors gratefully acknowledge the technical support of the UCLouvain LACAMI platform. Sanjay C Krishnamurthy is a FRIA grantee of the Belgian National Fund for Scientific Research (FNRS) and gratefully acknowledges their support. Hosni Idrissi is mandated by the Belgian National Fund for Scientific Research (FSR- FNRS). HR-TEM equipment used in the study has been funded by the FRS-FNRS INFRA-GEQ call 2021. The publication was supported by a grant from the Fondation Universitaire (Belgium).

Appendix A. Supplementary data

Supplementary data to this article can be found online at https://doi.org/10.1016/j.aime.2026.100191.

Data availability

Data will be made available on request.

References

Akisanya, A.R., Fleck, N.A., 1992. Brittle fracture of adhesive joints. Int. J. Fract. 58, 93–114. https://doi.org/10.1007/BF00019971.

Chen, Z.W., Yazdanian, S., 2015. Microstructures in interface region and mechanical behaviours of friction stir lap Al6060 to Ti–6Al–4V welds. Mater. Sci. Eng., A 634, 37–45. https://doi.org/10.1016/j.msea.2015.03.017.

Correia, A.N., Braga, D.F.O., Moreira, P.M.G.P., Infante, V., 2021. Review on dissimilar structures joints failure. Eng. Fail. Anal. 129. https://doi.org/10.1016/j.engfailanal.2021.105652.

Cozzolino, L.D., Coules, H.E., Colegrove, P.A., Wen, S., 2017. Investigation of post-weld rolling methods to reduce residual stress and distortion. J. Mater. Process. Technol. 247, 243–256. https://doi.org/10.1016/j.jmatprotec.2017.04.018.

DebRoy, T., Khan, K., Mukherjee, T., Zhang, W., Francis, J.A., De, A., 2026. Residual stress and distortion in fusion welding and fusion-based additive manufacturing: measurements, mechanisms and control strategies. Prog. Mater. Sci. 159, 101651. https://doi.org/10.1016/j.pmatsci.2025.101651.

Dezellus, O., Zhe, M., Gardiola, B., Lay, S., Viala, J.C., 2021. Solid state chemical interaction between Ti and Al-Si alloys. J. Phase Equilibria Diffus. 42, 524–534. https://doi.org/10.1007/s11669-021-00914-9.

Eisazadeh, H., Aidun, D.K., 2017. Investigation of transient/residual strain and stress in dissimilar weld. J. Manuf. Process. 26, 372–381. https://doi.org/10.1016/j.jmapro.2017.03.003.

Fernandes, F.A.O., Gonçalves, J.J.M., Pereira, A.B., 2023. Evaluation of laser lap weldability between the titanium alloy Ti-6Al-4V and aluminum alloy 6060-T6. Crystals 13, 1448. https://doi.org/10.3390/cryst13101448.

Froes, F.H., 1994. Advanced metals for aerospace and automotive use. Mater. Sci. Eng., A 184, 119–133. https://doi.org/10.1016/0921-5093(94)91026-X.

Fuji, A., Kimura, M., North, T.H., Ameyama, K., Aki, M., 1997. Mechanical properties of titanium-5083 aluminium alloy friction joints. Mater. Sci. Technol. 13, 673–678. https://doi.org/10.1179/mst.1997.13.8.673.

Gadakh, V.S., Badheka, V.J., Mulay, A.S., 2021. Solid-state joining of aluminum to titanium: a review. Proc. Inst. Mech. Eng., Part L 235, 1757–1799. https://doi.org/10.1177/14644207211010839.

Gaikwad, V.T., Mishra, M.K., Tripathi, A., Singh, R.K.P., 2024. On the role of upset pressure during friction welding of IN713LC and AISI 4140. Mater. Sci. Technol. https://doi.org/10.1177/02670836241273483.

Grassel, F., Malaske, L., Hoffmann, M., Klusemann, B., 2025. (semi-)solid-state joining of aluminium and titanium alloys – a critical review. J. Mater. Res. Technol. 39, 3270–3291. https://doi.org/10.1016/j.jmrt.2025.09.239.

Heidarzadeh, A., Mironov, S., Kaibyshev, R., Çam, G., Simar, A., Gerlich, A., Khodabakhshi, F., Mostafaei, A., Field, D.P., Robson, J.D., Deschamps, A., Withers, P.J., 2021. Friction stir welding/processing of metals and alloys: a comprehensive review on microstructural evolution. Prog. Mater. Sci. 117, 100752. https://doi.org/10.1016/j.pmatsci.2020.100752.

Jacques, P., van der Rest, C., Simar, A., 2012. Method for Welding at Least Two Layers.

Jain, S., Bhuva, K., Patel, P., Badheka, V.J., 2019. A review on dissimilar friction stir welding of aluminum alloys to titanium alloys. In: Advances in Intelligent Systems and Computing. Springer Verlag, pp. 415–425. https://doi.org/10.1007/978-981-13-1966-2_37.

Jiang, P., Chen, R., 2019. Research on interfacial layer of laser-welded aluminum to titanium. Mater. Charact. 154, 264–268. https://doi.org/10.1016/j.matchar.2019.06.012.

Jimenez-Mena, N., 2018. Optimization of the Friction Melt Bonding of Aluminium and Steel : from Microstructure Evolution to Mechanical Properties hdl.handle.net/2078.1/198376.

Jimenez-Mena, N., Jacques, P.J., Drezet, J.M., Simar, A., 2018. On the prediction of hot tearing in al-to-steel welding by friction melt bonding. Metall. Mater. Trans. A Phys. Metall. Mater. Sci. 49, 2692–2704. https://doi.org/10.1007/s11661-018-4618-z.

Jimenez-Mena, N., Sapanathan, T., Drezet, J.M., Pirling, T., Jacques, P.J., Simar, A., 2019. Residual stresses of friction melt bonded aluminum/steel joints determined by neutron diffraction. J. Mater. Process. Technol. 266, 651–661. https://doi.org/10.1016/j.jmatprotec.2018.11.030.

Jimenez-Mena, N., Sapanathan, T., Jacques, P.J., Simar, A., 2021. Combined numerical and experimental estimation of the fracture toughness and failure analysis of single lap shear test for dissimilar welds. Eng. Fract. Mech. 249, 107756. https://doi.org/10.1016/j.engfracmech.2021.107756.

Jonckheere, C., de Meester, B., Denquin, A., Simar, A., 2013. Torque, temperature and hardening precipitation evolution in dissimilar friction stir welds between 6061-T6 and 2014-T6 aluminum alloys. J. Mater. Process. Technol. 213, 826–837. https://doi.org/10.1016/j.jmatprotec.2013.01.001.

Karfoul, M.K., Tatlock, G.J., 2019. Interfacial processes during diffusion welding of titanium alloy/aluminium couples under ambient atmosphere. Weld. World 63, 841–849. https://doi.org/10.1007/s40194-019-00711-6.

Li, P., Lei, Z., Zhang, X., Chen, Y., 2020. Influence of Si content on interfacial reactions and mechanical properties of dual-spot laser welded-brazed Ti/Al joints. J. Manuf. Process. 56, 950–966. https://doi.org/10.1016/j.jmapro.2020.06.001.

Li, Y., Pang Ng, H., Jung, H. Do, Kim, H.E., Estrin, Y., 2014. Enhancement of mechanical properties of grade 4 titanium by equal channel angular pressing with billet encapsulation. Mater. Lett. 114, 144–147. https://doi.org/10.1016/j.matlet.2013.09.118.

Li, Y., Zhang, Y., Luo, Z., 2015. Microstructure and mechanical properties of Al/Ti joints welded by resistance spot welding. Sci. Technol. Weld. Join. 20, 385–394. https://doi.org/10.1179/1362171815Y.0000000028.

Liu, M., Zhang, C., Meng, Z., Zhao, G., Chen, L., 2022. Atomic diffusion mechanism and interface nanomechanics in the Al/Ti composite structures. Compos. B Eng. 230, 109507. https://doi.org/10.1016/j.compositesb.2021.109507.

Liu, M., Zhang, C., Meng, Z., Zhao, G., Chen, L., 2021. TiAl3 nucleation mechanism and atomic-scale interface features in the Al/Ti composite structures. Compos. B Eng. 226, 109331. https://doi.org/10.1016/j.compositesb.2021.109331.

Nan, X., Zhao, H., Jia, B.-B., Ma, C., Sun, G., Zhou, L., Wang, R., Song, X., 2025. The effect of rotational speed on microstructure and mechanical properties of Al/Ti dissimilar joint produced by refill friction stir spot welding. J. Mater. Eng. Perform. 34, 1812–1824. https://doi.org/10.1007/s11665-023-08545-6.

Özel, A., Aydin, M., Temiż, Ş., 2004. The effects of overlap length and adherend thickness on the strength of adhesively bonded joints subjected to bending moment. J. Adhes. Sci. Technol. 18, 313–325. https://doi.org/10.1163/156856104773635454.

Plaine, A.H., Gonzalez, A.R., Suhuddin, U.F.H., dos Santos, J.F., Alcântara, N.G., 2015. The optimization of friction spot welding process parameters in AA6181-T4 and Ti6Al4V dissimilar joints. Mater. Des. 83, 36–41. https://doi.org/10.1016/j.matdes.2015.05.082.

Pragana, J.P.M., Sampaio, R.F.V., Bragança, I.M.F., Silva, C.M.A., Martins, P.A.F., 2021. Hybrid metal additive manufacturing: a state–of–the-art review. Adv. Indus. Manuf. Eng. 2, 100032. https://doi.org/10.1016/j.aime.2021.100032.

Pretorius, R., Vredenberg, A.M., Saris, F.W., de Reus, R., 1991. Prediction of phase formation sequence and phase stability in binary metal-aluminum thin-film systems using the effective heat of formation rule. J. Appl. Phys. 70, 3636–3646. https://doi.org/10.1063/1.349211.

Ren, S., Ma, N., Tsutsumi, S., Watanabe, G., He, H., Cao, C., Huang, L., 2022. Post-weld cold working for fatigue strength improvement of resistance spot welded joint of advanced high-strength steel. J. Mater. Process. Technol. 299. https://doi.org/10.1016/j.jmatprotec.2021.117364.

Robson, J.D., 2020. Deformation enhanced diffusion in aluminium alloys. Metall. Mater. Trans. 51, 5401–5413. https://doi.org/10.1007/s11661-020-05960-5.

Simar, A., Avettand-Fènoël, M.-N., 2017. State of the art about dissimilar metal friction stir welding. Sci. Technol. Weld. Join. 22, 389–403. https://doi.org/10.1080/13621718.2016.1251712.

Soni, R., Verma, R., Kumar Garg, R., Sharma, V., 2024. A critical review of recent advances in the aerospace materials. Mater. Today Proc. 113, 180–184. https://doi.org/10.1016/j.matpr.2023.08.108.

Sujata, M., Bhargava, S., Sangal, S., 1997. On the formation of TiAl3 during reaction between solid Ti and liquid Al. J. Mater. Sci. Lett. 16, 1175–1178. https://doi.org/10.1007/BF02765402.

Van Der Rest, C., Jacques, P.J., Simar, A., 2014. On the joining of steel and aluminium by means of a new friction melt bonding process. Scr. Mater. 77, 25–28. https://doi.org/10.1016/j.scriptamat.2014.01.008.

Vyas, H.D., Mehta, K.P., Badheka, V., Doshi, B., 2021. Processing and evaluation of dissimilar Al-SS friction welding of pipe configuration: nondestructive inspection, properties, and microstructure. Measurement 167, 108305. https://doi.org/10.1016/j.measurement.2020.108305.

Xue, X., Wu, X., Liao, J., 2021. Hot-cracking susceptibility and shear fracture behavior of dissimilar Ti6Al4V/AA6060 alloys in pulsed Nd:YAG laser welding. Chin. J. Aeronaut. 34, 375–386. https://doi.org/10.1016/j.cja.2020.12.015.

Zhang, C., Robson, J.D., Haigh, S.J., Prangnell, P.B., 2019. Interfacial segregation of alloying elements during dissimilar ultrasonic welding of AA6111 aluminum and Ti6Al4V titanium. Metall. Mater. Trans. A Phys. Metall. Mater. Sci. 50, 5143–5152. https://doi.org/10.1007/s11661-019-05395-7.

Zhang, C.Q., Robson, J.D., Prangnell, P.B., 2016. Dissimilar ultrasonic spot welding of aerospace aluminum alloy AA2139 to titanium alloy TiAl6V4. J. Mater. Process. Technol. 231, 382–388. https://doi.org/10.1016/j.jmatprotec.2016.01.008.

Zheng, Z.-M., Zhang, J., Xing, Y.-Z., 2025. A review on controlling the formation of intermetallic compounds in Ti/Al dissimilar metal laser weld seams. Weld. World. https://doi.org/10.1007/s40194-025-02198-w.